Journal of Materials Chemistry A

RSC Publishing

PAPER

View Article Online
View Journal | View Issue

Cite this: J. Mater. Chem. A, 2013, 1, 2896

Influence of intrinsic oleophobicity and surface structuration on the superoleophobic properties of PEDOP films bearing two fluorinated tails

Herve Bellanger, Thierry Darmanin, Elisabeth Taffin de Givenchy and Frederic Guittard*

Received 1st October 2012
Accepted 10th December 2012

DOI: 10.1039/c2ta00517d

www.rsc.org/MaterialsA

Here, we report the synthesis and characterization of original 3,4-ethylenedioxypyrrole derivatives bearing two fluorinated tails (*F*-butyl: EDOP$(F_4)_2$ and *F*-hexyl: EDOP$(F_6)_2$). These monomers are used for the elaboration of superoleophobic surfaces by electrodeposition of conducting polymers. Cyclic voltammetry experiments show high steric hindrances during the electropolymerization due to the presence of the two fluorinated chains. Using a constant potential as deposition method, superhydrophobic and oleophobic surfaces are obtained ($\theta_{hexadecane} = 110.1°$ and 89.3° for PEDOP$(F_6)_2$ and PEDOP$(F_4)_2$, respectively). To improve the surface oleophobicity, various deposition methods were used. Superoleophobic surfaces with $\theta_{hexadecane} \approx 140°$ are obtained with PEDOP$(F_6)_2$ using galvanostatic deposition (0.5 mA cm^{-2}) and pulse potentiostatic deposition (t_p/t_r: 9 s/5 s). The superoleophobic properties are in part due to the presence of both surface microstructures and nanoporosities. In order to determine the influence of the intrinsic oleophobicity and surface structuration on the static contact angle of various probe liquids, from octane ($\gamma_{LV} = 21.6$ mN m^{-1}) to water ($\gamma_{LV} = 72.8$ mN m^{-1}), smooth surfaces were prepared. Here, surprisingly, a very important increase in surface oleophobicity is observed for all the tested probe liquids even if the contact angle of the smooth surface is much lower than 90° (*e.g.*: for octane, an increase from 57.4 to 107.0 was observed after surface structuration, for the best surface). This is in total contradiction with the Wenzel theory but can be explained by the presence of re-entrant structures, as described in the literature. This work confirms the importance of surface nanoporosities for the repellency of low surface tension liquids such as oils.

1 Introduction

The development of superoleophobic surfaces, which repel low surface tension liquids such as oils, is in constant evolution due to their high potential applications in antifingerprint touch sensitive screens[1] and optical devices,[2] water–oil separation,[3] oil transportation,[4] microfluidic channels,[5] resistant ink jet print heads,[6] oil stain-resistant fabrics[7] and military uniforms protected against hazardous chemicals.[8] In a theoretical point of view and to find new strategies to produce such surfaces, it has been extremely indispensable to understand how to repel low surface tension liquids. Such surface properties come from the elaboration of superhydrophobic surfaces, which combine low surface energy materials and surface roughness.[9–11] In the case of superhydrophobic surfaces, Wenzel and Cassie–Baxter theories are very often used to predict such properties.[12,13] According to these two theories, surface roughness can increase the surface hydrophobicity of intrinsically hydrophobic materials.

In order to explain the possibility to reach superhydrophobic surfaces from intrinsically hydrophilic materials, many efforts were dedicated to the adaptation of these theories.[14,15] Indeed, many works reported, under certain conditions, clear deviations of these theories in comparison to experimental conditions.[16] Many authors showed that the presence at the surface of structures having particular geometries, named overhanging or re-entrant structures, can induce this effect. For example, the group of Liu showed that the key parameter to be in the Cassie–Baxter state using hydrophilic materials is the change in the angle, from concave to convex, between re-entrant structures, which can induce a negative Laplace pressure difference.[15b] Author groups showed that the presence of re-entrant structures induces the formation of capillary forces that prevent water from entering these structures, creating an energy barrier separating the Cassie–Baxter state and the Wenzel one. As a consequence, the water droplet is in a metastable Cassie–Baxter state.[15c,d,16c]

Université de Nice – Sophia Antipolis & CNRS, Laboratoire de Physique de la Matière Condensée, Groupe Surfaces & Interfaces, Parc Valrose, 06108 Nice Cedex 2, France. E-mail: Frederic.GUITTARD@unice.fr; Fax: +33 4-92-07-61-56; Tel: +33 4-92-07-61-59

Because even fluorinated materials are not sufficiently intrinsically oleophobic (*e.g.*: for smooth PTFE, the contact angle of water ≈ 110° while that of hexadecane ≈ 40° or octane ≈ 25°) to produce superoleophobic surfaces just by increasing the surface roughness, it was necessary to produce superoleophobic surfaces from intrinsically oleophilic materials. Hence, such materials are derived from the elaboration of superhydrophobic surfaces using hydrophilic materials. Indeed, the group of McKinley demonstrated the possibility to produce superoleophobic surfaces by combining re-entrant curvatures with fluorinated materials.[17] Moreover, by analyzing the three-phase contact line displacement, the validity of the Cassie–Baxter theory for obtaining superoleophobic surfaces using re-entrant structures was also reported.[18]

Until now, the elaboration of superoleophobic surfaces was reported by combining low surface energy materials as re-entrant structures, such as mushroom-like structures, oblique and curved 3D microstructures or nanonails.[19–26] Superoleophobic surfaces could be obtained on various substrates by two general approaches: top down methods, where the substrate usually has to be coated with low surface energy materials after being etched, or bottom up approaches, where the surface structuration can be obtained along with the substrate coating. In this last method, the low surface energy material can be the coating itself or it can be brought in by an additional coating step. This last approach is the most interesting because it is generally easier to perform, as it involves spraying or deposition of particles in solution.

Electrochemical polymerization of conducting polymers is one of them. Highly oleophobic surfaces were obtained by Tsujii *et al.* by, for example, the electrodeposition of poly(*N*-alkylpyrrole) followed by coating with fluorinated compounds.[27] Another approach was to graft a fluorinated chain on the monomer to lower the surface energy of the resulting polymer and suppress the last coating step.[19,28,29] 3,4-Ethylenedioxypyrrole bearing a *F*-hexyl or *F*-octyl side chain showed exceptional superoleophobic properties, with contact angles up to 150° with hexadecane, and very low hysteresis could be achieved.[19]

In this work, our approach was to try to decrease the surface energy and to control the surface structuration, which are two parameters that govern wettability properties. The common approach to decrease surface energy is to increase the length of the fluorinated tail. But such long chains are bioaccumulable and thus we should explore ways to replace them.[30–33] One of the challenges in superoleophobic surface development is thus the use of short fluorinated chains. For that purpose, we synthesized original 3,4-ethylenedioxypyrrole monomers bearing two fluorinated tails (*F*-hexyl and *F*-butyl), represented in Scheme 1 (EDOP(F_n)$_2$), in order to increase the number of $-CF_2$ and $-CF_3$ groups per monomer unit without increasing the length of the fluorinated chains. To synthesize these monomers, a novel EDOP synthon functionalized with two hydroxyl groups was successfully obtained (Scheme 1; EDOP(OH)$_2$). For the control of surface structuration, we exploited the ability of conductive polymers to grow differently depending on the used deposition method. Indeed, the electropolymerization conditions may have a high influence on the structuration of the resulting polymer film.[34,35] Here, the monomers were electropolymerized by galvanostatic, potentiostatic and pulse potentiostatic methods. The surface morphology, roughness, electrochemical properties and wetting properties were analyzed by scanning electron microscopy, optical profilometry, cyclic voltammetry and contact angle (static and dynamic) measurements with water and hexadecane droplets as liquid probes for hydrophobicity and oleophobicity.

2 Experimental

3,4-Ethylenedioxypyrrole (EDOP) was synthesized in eight steps from iminodiacetic acid.[36] The original molecule EDOP(OH)$_2$, containing two hydroxyl groups, was synthesized by adapting the reaction reported for the preparation of hydroxyalkylpyrrole: synthesis at room temperature in DMSO using KOH as the base and 3-chloro-1,2-propanediol as the reagent.[37] Finally, the monomers EDOP(F_n)$_2$ were successfully obtained using 3-*F*-alkylethanoic acids with *N*-(3-dimethylaminopropyl)-*N*′-ethylcarbodiimide hydrochloride (EDC) and 4-dimethylaminopyridine (DMAP) as coupling agents at room temperature.

2.1 Synthesis of 3-(2*H*-[1,4]dioxino[2,3-*c*]pyrrol-6(3*H*)-yl) propane-1,2-diol (EDOP(OH$_2$))

EDOP (6 eq., 560 mg, 4.48 mmol) was added to a suspension of KOH (4 eq., 167 mg, 2.98 mmol) in DMSO (7.5 mL). The reaction mixture was stirred for one hour and cooled in an ice bath before dropwise addition of a solution of 3-chloro-1,2-propanediol (1 eq., 82 mg, 0.75 mmol) in DMSO (1.5 mL). After stirring at room temperature for 24 h, water was added and the product was extracted with dichloromethane. The combined organic phases were washed with brine and dried over sodium sulphate. Evaporation of the solvent and column chromatography purification (silica gel, cyclohexane/ethyl acetate 1 : 1) gave the product as a yellow oil.

EDOP(OH)$_2$. Yield 51%; rt 13.7 min; yellow oil; δ_H(200 MHz, $CDCl_3$): 6.09 (2H, s), 4.14 (4H, s), 3.70 (5H, m), 3.21 (1H, s), 2.99 (1H, s); δ_C(200 MHz, $CDCl_3$): 132.30, 101.75, 71.79, 65.75, 63.68, 52.63; MS (70 eV): *m*/*z* 199 (M^+, 100), 138 ($C_7H_8NO_2^+$, 47), 112 ($C_5H_6NO_2^+$, 99); FTIR (KBr): ν_{max}/cm^{-1} 3405, 2913, 1641, 1499, 1316, 1054, 768 cm^{-1}.

2.2 Synthesis of EDOP(F_n)$_2$

The corresponding semifluorinated acid (2.5 mmol), EDC (2.5 mmol) and DMAP (40 mg) were added to 20 mL of dichloromethane. After stirring for 30 min at room temperature, EDOP(OH)$_2$ (1.0 mmol) was added. After stirring for a day at 50 °C, the solvent was removed and the crude was purified by column chromatography (silica gel; eluent) to yield the products.

3-(2*H*-[1,4]Dioxino[2,3-*c*]pyrrol-6(3*H*)-yl)propane-1,2-diyl bis(4,4,5,5,6,6,7,7,7-nonafluoroheptanoate) (EDOP(F_4)$_2$). Yield 66%; rt 19.0 min; oil; δ_H(200 MHz, $CDCl_3$): 6.04 (2H, s), 5.22 (1H, m), 4.35 (1H, dd, *J* 12.16, *J* 3.46), 4.16 (4H, s), 3.97 (1H, dd, *J* 12.16, *J* 5.62), 3.87 (2H, d, *J* 6.04), 2.63 (8H, m); δ_C(50 MHz,

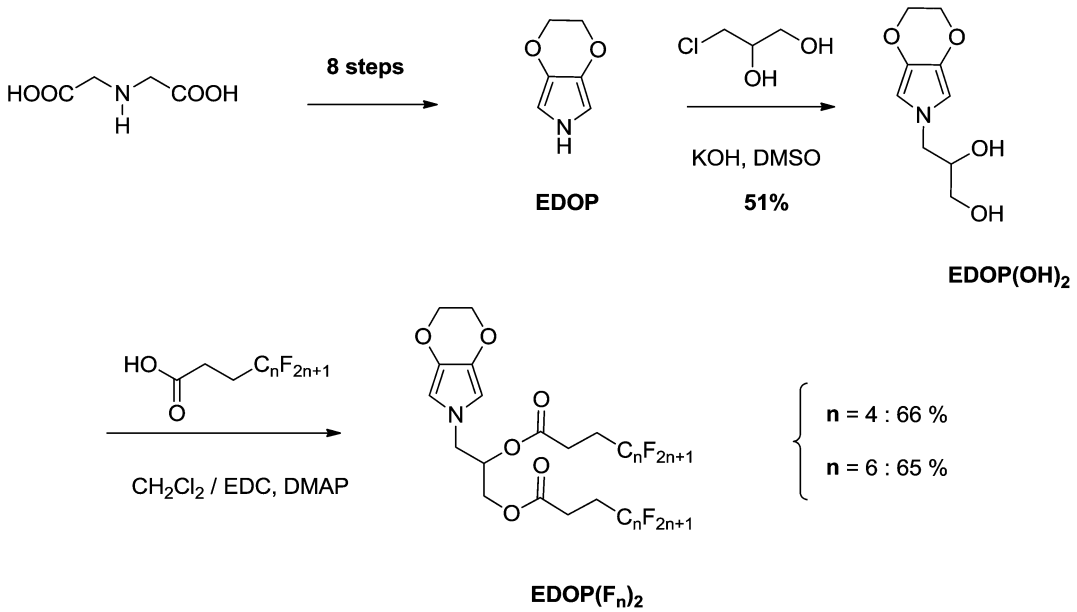

Scheme 1 Synthetic route to the monomers EDOP(F_n)$_2$.

$CDCl_3$): 170.65, 170.22, 132.75, 101.78, 71.33, 65.72, 62.92, 49.60, 29.69, 26.26, 25.84, 25.33; δ_F(188 MHz, $CDCl_3$): −80.08 (6F, m), −115.10 (4F, m), −124.57 (4F, m), − 126.14 (4F m); EIMS: *m*/*z* 786 (M + K).

3-(2*H*-[1,4]Dioxino[2,3-*c*]pyrrol-6(3*H*)-yl)propane-1,2-diyl bis-(4,4,5,5,6,6,7,7,8,8,9,9,9-tridecafluorononanoate) (EDOP(F_6)$_2$). Yield 65%; rt 20.5 min; oil; δ_H(200 MHz, $CDCl_3$): 6.04 (2H, s), 5.22 (1H, m), 4.36 (1H dd, *J* 12.16, *J* 3.36), 4.16 (4H s), 3.96 (1H, dd, *J* 12.16, *J* 5.70), 3.87 (2H, d, *J* 6.05), 2.63 (8H, m); δ_C(50 MHz, $CDCl_3$): 170.67, 170.23, 132.75, 101.78, 71.33, 65.72, 62.92, 49.60, 29.69, 26.35, 25.27; δ_F(188 MHz, $CDCl_3$): −80.87 (6F, m), −114.91 (4F, m), −122.02 (4F, m), −123.01 (4F, m), −123.64 (4F, m), −126.25 (4F, m), EIMS: *m*/*z* 986 (M + K).

3 Results and discussion

3.1 Electrodeposition and cyclic voltammetry study

To electrodeposit the polymers, it was first necessary to determine the monomer oxidation potential because monomer oxidation, polymerization and polymer deposition take place at this potential. Since this oxidation potential is dependent on electrochemical parameters, in our work the deposition was performed in anhydrous acetonitrile and using tetrabutylammonium hexafluorophosphate (Bu_4NPF_6; 0.1 M) as the electrolyte. The used system consisted of a three-electrode system: a platinum disk working electrode, a graphite bar counter-electrode and a saturated calomel reference electrode (SCE). An oxidation potential of 1.08 V and 1.05 V was determined by cyclic voltammetry (0.2 V s^{-1}) for EDOP(F_6)$_2$ and for EDOP(F_4)$_2$, respectively.

The determination of this oxidation potential being not sufficient to assure the growth of a polymer film on the working electrode, this growth was then studied by performing multiple scans by cyclic voltammetry from −1 V until a potential slightly lower than the monomer oxidation potential. The cyclic voltammograms of the electrodeposition of the two monomers are given in Fig. 1a and c. The increase of the intensity of the polymer oxidation peak after each scan confirms the formation of polymer layers. In the case of EDOP(F_4)$_2$, after each scan, the polymer oxidation potential is linearly shifted to higher potentials. Indeed, it seems that the presence of two *F*-butyl chains induced significant steric hindrances during the polymerization and that the mean conjugation length decreases after each scan. This effect was drastic in the case of EDOP(F_6)$_2$, as shown in Fig. 1c.

After deposition, the electrode covered with the deposited film was rinsed and transferred to a monomer free solution and 10 scans were performed to identify the polymer redox system. For both PEDOP(F_4)$_2$ and PEDOP(F_6)$_2$, each scan was superimposable which revealed a high stability of the polymer films. As shown in Fig. 1b and d, single redox couples were identified on both polymers. Although oxidation potentials of the two monomers are similar, a huge difference was observed between oxidation potentials ($E_{ox,p}$) of PEDOP(F_4)$_2$ and PEDOP(F_6)$_2$ which were respectively 0.39 V and 0.74 V. This high shift revealed that the conjugation length of PEDOP(F_6)$_2$ polymer chains is much lower than that of PEDOP(F_4)$_2$. This can be explained by the higher steric hindrance induced by two long *F*-hexyl tails.

3.2 Surface properties of films produced at constant potential

To determine the surface properties, it was necessary to replace the platinum tip with larger gold plates as working electrodes. The anti-liquid properties were evaluated with two liquid probes of different surface tensions: water (72.8 mN m^{-1}) and hexadecane (27.6 mN m^{-1}) for the determination of

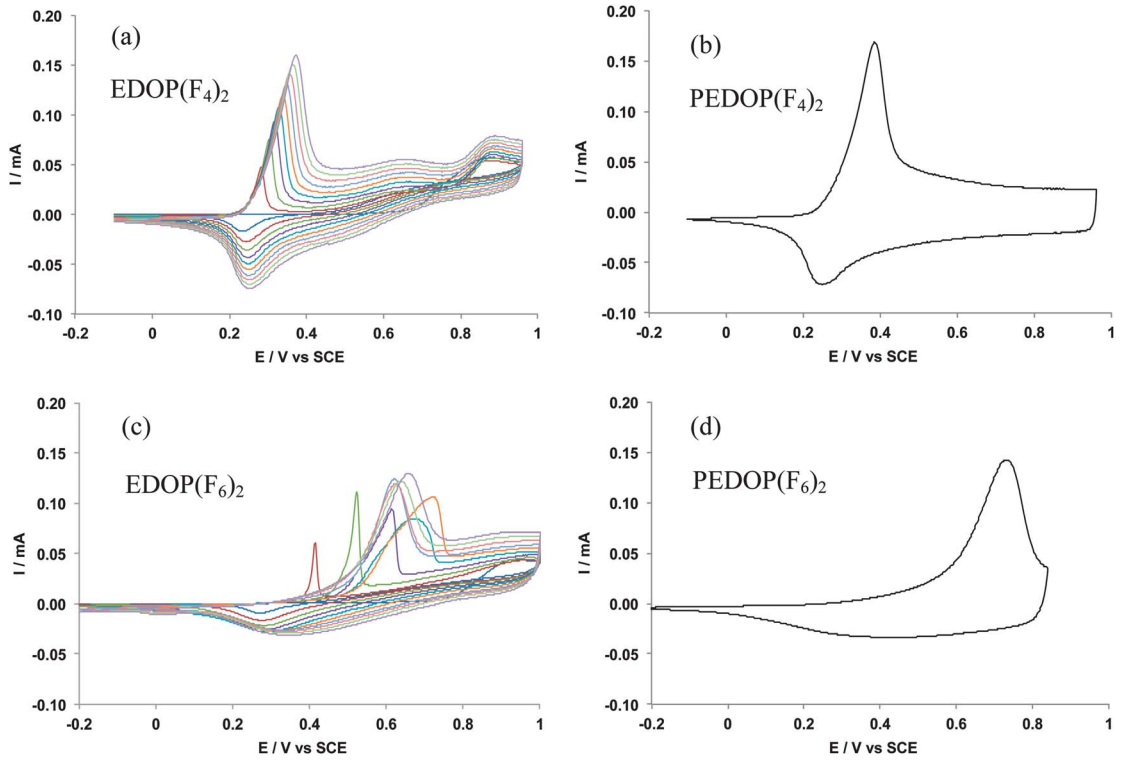

Fig. 1 Deposition by CV of (a) EDOP$(F_4)_2$ and (c) EDOP$(F_6)_2$ and CV of (b) PEDOP$(F_4)_2$ and (d) PEDOP$(F_6)_2$ recorded in 0.1 M Bu_4NPF_6 and anhydrous acetonitrile.

superhydrophobic and superoleophobic properties, respectively. First, the deposition was performed at 1000 mV, a potential slightly lower than the oxidation potential of the monomer, and various deposition charges from 25 mC cm^{-2} to 400 mC cm^{-2}. For PEDOP$(F_6)_2$, the films were superhydrophobic with a low sliding angle and hysteresis for a deposition charge of 225 mC cm^{-2} ($\theta_{water} = 159.7°$, $\alpha_{water} = 1.5°$ and $H_{water} = 5°$). A higher deposition charge of 400 mC cm^{-2} was necessary to reach superhydrophobic properties with PEDOP$(F_4)_2$ but with a much higher adhesion. Indeed, water droplets could be removed on PEDOP$(F_6)_2$ surfaces with a slight surface inclination while on PEDOP$(F_4)_2$ the water droplets remained stuck even for a surface inclination of 90°. These two effects can be explained with the Cassie–Baxter and Wenzel theories.[12,13] Indeed, on PEDOP$(F_6)_2$ surfaces, a water droplet is in the Cassie–Baxter state (high θ and low H), which means that the presence of air pockets makes the suspension of the water droplet easier due to the presence of liquid–vapor interfaces. On PEDOP$(F_4)_2$ surfaces, the water droplet is in contact with all the surface (Wenzel state), which increases the static contact angle but also the adhesion of the water droplet (high hysteresis).

However, these two polymers were not superoleophobic with $\theta_{hexadecane} = 110.1°$ and 83.4°, for PEDOP$(F_6)_2$ and PEDOP$(F_4)_2$, respectively. $\theta_{hexadecane}$ was lower than those measured on surfaces obtained from EDOP derivatives containing a single fluorinated chain.[19b] Hence, to understand these differences in surface wettability, SEM images were obtained for these surfaces.

SEM analyses revealed that the surface morphology of PEDOP$(F_4)_2$ presented stacking of smooth spherical particles with diameter from submicrometer to about 5 μm on a leveled layer (Fig. 2a). Hence, this polymer was not superoleophobic because the microstructures are too smooth to reach such properties. By contrast, PEDOP$(F_6)_2$ presented micro and nanostructured surfaces close to cauliflower-like structures (Fig. 2b). These structures led to higher oleophobicity but this surface morphology was also not sufficient to reach superoleophobic properties.

3.3 Influence of the deposition method on surface oleophobicity

In order to improve the surface oleophobicity of the films, other electrochemical conditions and methods were performed. First of all, whatever the deposition method, PEDOP$(F_4)_2$ films were always oleophilic meaning that the study of different deposition methods did not allow us to improve the surface oleophobicity of PEDOP$(F_4)_2$. For PEDOP$(F_6)_2$, we first adopted the same deposition method but studied the influence of the polymerization potential (from 0.89 V to 1.05 V). Fig. 3 shows the influence of the deposition potential on the oleophobic properties. The best results were obtained for a deposition potential of 0.95 V but the increase in oleophobicity was not highly significant.

For the galvanostatic deposition method, the current density range was determined to be from 0.10 mA cm^{-2} to 0.70 mA cm^{-2}. Those values of current density allowed reaching a plateau at a potential close to the polymerization potential. Lower current density would lead to very long deposition times and at higher current density, the potential increased over the

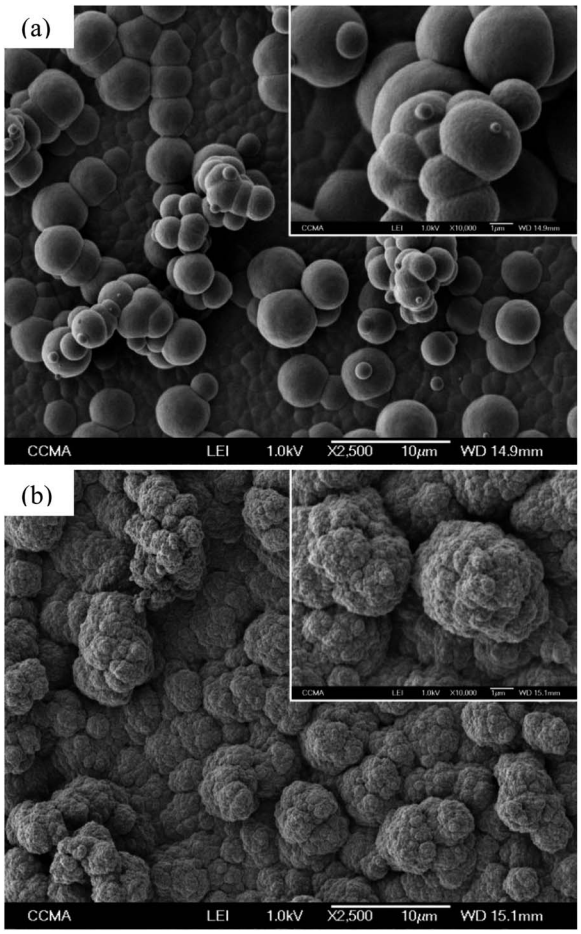

Fig. 2 SEM images of (a) PEDOP$(F_4)_2$ and (b) PEDOP$(F_6)_2$; Qs = 225 mC cm^{-2}.

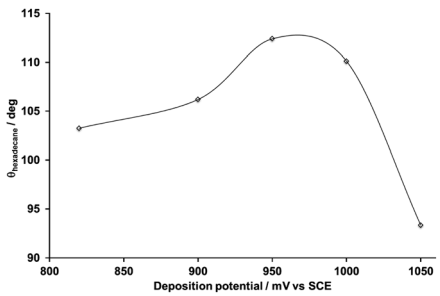

Fig. 3 Contact angle of hexadecane as a function of the deposition potential for PEDOP$(F_6)_2$.

oxidation potential without stabilizing, which is not desired for polymerization. For galvanostatic deposition at 0.10 mA cm^{-2} and 0.30 mA cm^{-2}, the polymer did not homogeneously cover the substrate and the contact angle measurement would not be relevant. Surprisingly, at 0.50 mA cm^{-2} the films were homogeneous and superoleophobic properties were reached with a very high $\theta_{hexadecane}$ of 140.7°.

Polymer films were also electrodeposited by pulse potentiostatic programs using the following cycles: 9 s at 1.00 V (polymerization time, t_p) and 5 s at 0.00 V (relaxing time, t_r) or 2 s at 1.00 V and 5 s at 0.00 V. 50 cycles were performed for a deposition time of 400 s. Interestingly, the use of a long potential pulse (9 s) at 1.00 V could increase the contact angle up to 135.2°, while a short potential pulse (2 s) did not improve the surface oleophobicity. Here the deposition charge could not be directly determined during the experiment because of the discharging effect during the relaxing period. Profilometry analyses showed that the electrodeposition of PEDOP$(F_6)_2$ provided films of similar roughness profiles for potentiostatic deposition (Ra = 2.59 μm), galvanostatic deposition (Ra = 2.54 μm) and pulse potentiostatic deposition (9 s/5 s) (Ra = 2.57 μm). Hence, the high values of $\theta_{hexadecane}$ of 140.7° and 135.2° respectively measured with films grown by galvanostatic and pulse potentiostatic methods, compared to $\theta_{hexadecane}$ of 110.1° measured with the film grown by the potentiostatic method, could not be explained by roughness differences at a micro-scale. These differences are explained by differences observed in their surface morphology at a nano-scale. Indeed, nanoporosity was only observed on the films deposited by galvanostatic deposition and pulse potentiostatic deposition (9 s/5 s) as shown in Fig. 4. Here, the nanoporosity could induce the presence of re-entrant structures and as a consequence super-oleophobic surfaces were obtained, according to Choi's model.[18] However, after surface inclination, the hexadecane droplet remained stuck on the surface, which means that the

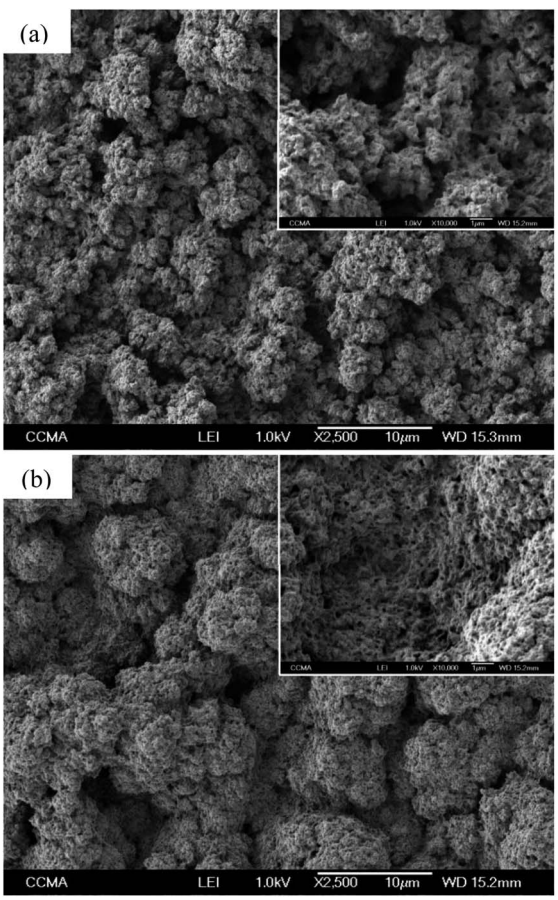

Fig. 4 SEM images of PEDOP$(F_6)_2$ deposited by (a) the galvanostatic method at 500 mA cm^{-2} and (b) pulse potentiostatic method (9 s).

droplet was not in the Cassie–Baxter state but in an intermediate state between the Wenzel and the Cassie–Baxter states.

Hence, the surface oleophobicity of PEDOP$(F_6)_2$ films produced by galvanostatic deposition (0.50 mA cm^{-2}) and pulse potentiostatic deposition (9 s/5 s) is relatively close to that of the previous PEDOP films containing a single fluorinated tail and electrodeposited at a constant potential. Indeed, the key parameter to produce superoleophobic surfaces is the surface morphology and in our work the presence of surface nanoporosity. This is in contrast to the expected decrease of surface energy due to the presence of two fluorinated chains.

Previously, it has also been demonstrated that the presence of surface nanoporosity may be due to a complex doping process, which is only possible if the planarity of the polymer is not too affected, by the presence of a substituent for example.[19a] In this work, the presence of two fluorinated chains induced very high steric hindrances, which impede the possibility to perform complex doping processes (only one oxidation peak observed by cyclic voltammetry) and the formation of surface nanoporosity. We suppose that the change in the deposition method and more precisely two deposition methods (galvanostatic deposition (0.50 mA cm^{-2}) and pulse potentiostatic deposition (9 s/5 s)) could slow down the polymer growth in comparison with the deposition at a constant potential, reduce the steric hindrances and by the same mechanism produce superoleophobic nanoporous films.

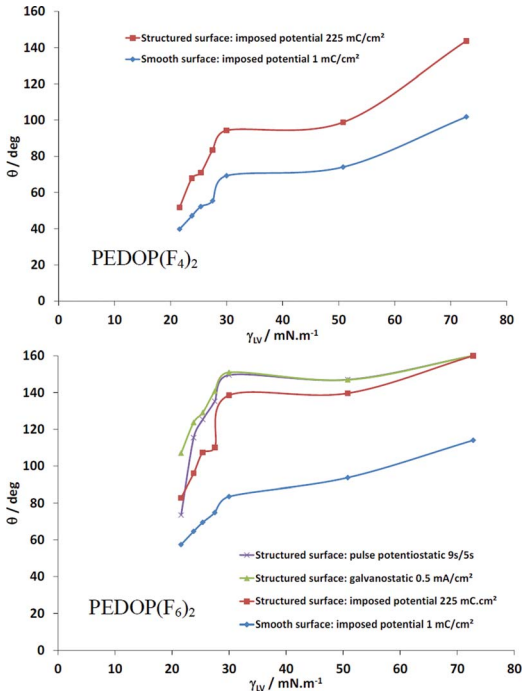

Fig. 5 Contact angle on smooth and structured surfaces, for PEDOP$(F_4)_2$ and PEDOP$(F_6)_2$, as a function of the liquid probe.

3.4 Influence of intrinsic oleophobicity and surface structuration on the surface oleophobicity

In order to determine the influence of intrinsic oleophobicity (chemical part), and as a consequence that of surface structuration (physical part), on the surface oleophobicity of the structured polymer films, smooth PEDOP$(F_4)_2$ and PEDOP$(F_6)_2$ films were produced reducing the deposition charge to 1 mC cm^{-2} (Ra < 10 nm). The contact angles of the smooth and the structured surfaces as a function of the surface tension of the probe liquid (γ_{LV}) are collected in Table 1 and Fig. 5. First of all, as expected, the intrinsic hydrophobicity and oleophobicity of PEDOP$(F_6)_2$ are higher than those of PEDOP$(F_4)_2$. Surprisingly, for PEDOP$(F_6)_2$ and PEDOP$(F_4)_2$, the contact angle of the smooth surfaces was always lower than that of the structured surfaces, even when the contact angle of the smooth surface was much lower than 90°, in total disagreement with the Wenzel theory. Hence, the presence of surface microstructures as well as surface nanoporosities observed for PEDOP$(F_4)_2$ and PEDOP$(F_6)_2$, respectively, induces the presence of re-entrant structures. For example, the contact angle of octane on PEDOP$(F_6)_2$ deposited by galvanostatic deposition was 107.0° while that of smooth PEDOP(F_6) was 57.4° and the Wenzel theory predicts a contact angle close to 0°.

From the contact angles of the smooth surface, the influence of the surface structuration could be detected. For example, the influence of these two parameters is given in Fig. 6 for PEDOP$(F_6)_2$ deposited by galvanostatic deposition. For this film, the influence of the surface structuration represented 44–48% from octane to sunflower oil and a little less after.

Table 1 Static contact angles for the structured and the smooth polymer surfaces

		PEDOP$(F_4)_2$		PEDOP$(F_6)_2$			
Probe liquid	γ_{LV} (mN m^{-1})	Smooth[a]	Imposed potential (225 mC cm^{-2})	Smooth[a]	Imposed potential (225 mC cm^{-2})	Galvanostatic (0.50 mA cm^{-2})	Pulse potentiostatic (9 s/5 s)
Water	72.8	101.8	143.7	114.0	159.7	160.0	160.0
Diiodomethane	50.8	74.0	98.8	93.7	139.6	146.9	147.0
Sunflower oil	30.0	69.2	94.3	83.5	138.5	151.0	149.5
Hexadecane	27.5	55.3	83.4	74.8	110.1	140.7	135.2
Dodecane	25.4	52.1	70.9	69.5	107.4	129.1	125.3
Decane	23.8	47.1	67.8	64.6	96.1	123.7	115.4
Octane	21.6	39.8	51.6	57.4	82.8	107.0	73.5

[a] Obtained by the imposed potential for Qs = 1 mC cm^{-2}.

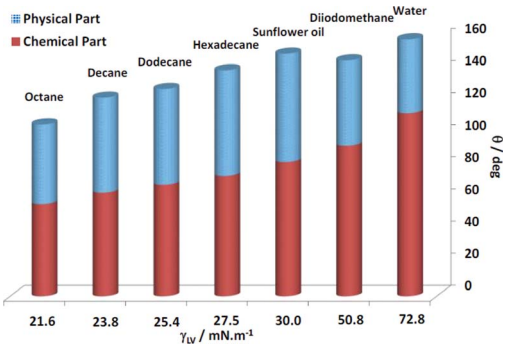

Fig. 6 Chemical and physical parts of the contact angle on PEDOP$(F_6)_2$ deposited by galvanostatic deposition (0.50 mA cm^{-2}) as a function of the liquid probe.

4 Conclusions

Here, we have shown the possibility to produce superoleophobic surfaces from original 3,4-ethylenedioxypyrrole derivatives containing two fluorinated chains. The electrodeposition at constant potential has led to superhydrophobic and oleophobic surfaces ($\theta_{hexadecane}$ = 110.1° and 89.3° for PEDOP$(F_6)_2$ and PEDOP$(F_4)_2$, respectively). In this work, the key parameter to obtain superoleophobic properties was found to be the presence of surface nanoporosities in the films. A study of the electrodeposition method has shown that galvanostatic deposition (0.50 mA cm^{-2}) and pulse potentiostatic deposition (9 s/5 s) are efficient methods to produce nanoporous superoleophobic surfaces using PEDOP$(F_6)_2$. The preparation of smooth surfaces allowed the determination of the influence of intrinsic oleophobicity and surface structuration on the static contact angle of various probe liquids, from octane to water. Surprisingly, for all the tested probe liquids, a very important increase in surface oleophobicity was observed, even if the contact angle of the smooth surface was much lower than 90°. This is in total contradiction with the Wenzel theory but can be explained by the presence of re-entrant structures, as described in the literature.

Notes and references

1 S. Jin and C. Choi, *PCT Int. Appl.*, WO 2012088209 A2 20120628, 2012.
2 S. Jin, C. Choi and K. Ogawa, *PCT Int. Appl.*, WO 2009078109 A1 20090625, 2009.
3 (*a*) X. Liu, J. Gao, Z. Xue, L. Chen, L. Lin, L. Jiang and S. Wang, *ACS Nano*, 2012, **6**, 5614; (*b*) A. Tuteja, A. K. Kota, G. Kwon and J. M. Mabry, *US Pat. Appl. Publ.*, US 20120000853 A1 20120105, 2012.
4 X. Yao, J. Gao, Y. Song and L. Jiang, *Adv. Funct. Mater.*, 2011, **21**, 4270.
5 D. Wu, S.-Z. Wu, Q.-D. Chen, S. Zhao, H. Zhang, J. Jiao, J. A. Piersol, J.-N. Wang, H.-B. Sun and L. Jiang, *Lab Chip*, 2011, **11**, 3873.
6 (*a*) P. M. Gulvin and H. Zhao, *US Pat. Appl. Publ.*, US 20110157278 A1 20110630, 2011; (*b*) K.-Y. Law and H. Zhao, *U.S. Pat. Appl. Publ.*, US 20090324308 A1 20091231, 2009.
7 (*a*) C. Pereira, C. Alves, A. Monteiro, C. Magen, A. M. Pereira, A. Ibarra, M. R. Ibarra, P. B. Tavares, J. P. Araujo, G. Blanco, J. M. Pintado, A. P. Carvalho, J. Pires, M. F. R. Pereira and C. Freire, *ACS Appl. Mater. Interfaces*, 2011, **3**, 2289; (*b*) X. Ye, *Faming Zhuanli Shenqing*, CN 102354058 A 20120215, 2012.
8 D. Satam, H. J. Lee and E. Wilusz, *AATCC Rev.*, 2010, **10**, 59.
9 (*a*) K. Liu, X. Yao and L. Jiang, *Chem. Soc. Rev.*, 2010, **39**, 3240; (*b*) M. Liu and L. Jiang, *Adv. Funct. Mater.*, 2010, **20**, 3753.
10 (*a*) Z. Guo, W. Liu and B.-L. Su, *J. Colloid Interface Sci.*, 2011, **353**, 335; (*b*) K. Liu and L. Jiang, *Nanoscale*, 2011, **3**, 825.
11 N. J. Shirtcliffe, G. McHale and M. I. Newton, *J. Polym. Sci., Part B: Polym. Phys.*, 2011, **49**, 1203.
12 R. N. Wenzel, *Ind. Eng. Chem.*, 1936, **28**, 988.
13 (*a*) A. B. D. Cassie and S. Baxter, *Trans. Faraday Soc.*, 1944, **40**, 546; (*b*) S. Baxter and A. B. D. Cassie, *J. Text. Inst., Trans.*, 1945, **36**, T67.
14 (*a*) S. Herminghaus, *Europhys. Lett.*, 2000, **52**, 165; (*b*) C. W. Extrand, *Langmuir*, 2002, **18**, 7991; (*c*) A. Marmur, *Langmuir*, 2008, **24**, 7573.
15 (*a*) L. Cao, T. P. Price, M. Weiss and D. Gao, *Langmuir*, 2008, **24**, 1640; (*b*) J.-L. Liu, X.-Q. Feng, G. Wang and S.-W. Yu, *J. Phys.: Condens. Matter*, 2007, **19**, 356002; (*c*) M. Nosonovsky, *Langmuir*, 2007, **23**, 3157; (*d*) L. Cao, H.-H. Hu and D. Gao, *Langmuir*, 2007, **23**, 4310.
16 (*a*) H. Y. Erbil and C. E. Cansoy, *Langmuir*, 2009, **25**, 14135; (*b*) C. E. Cansoy, H. Y. Erbil, O. Akar and T. Akin, *Colloids Surf., A*, 2011, **386**, 116; (*c*) K. Kurogi, H. Yan and K. Tsujii, *Colloids Surf., A*, 2008, **317**, 592.
17 A. Tuteja, W. Choi, M. Ma, J. M. Mabry, S. A. Mazzella, G. C. Rutledge, G. H. Mckinley and R. E. Cohen, *Science*, 2007, **318**, 1618.
18 W. Choi, A. Tuteja, J. M. Mabry, R. E. Cohen and G. H. Mckinley, *J. Colloid Interface Sci.*, 2009, **339**, 208.
19 (*a*) T. Darmanin and F. Guittard, *J. Am. Chem. Soc.*, 2009, **131**, 7928; (*b*) H. Bellanger, T. Darmanin and F. Guittard, *Langmuir*, 2012, **28**, 186.
20 H. Zhao, K.-Y. Law and V. Sambhy, *Langmuir*, 2011, **27**, 5927.
21 G. R. J. Artus, J. Zimmermann, F. A. Reifler, S. A. Brewer and S. Seeger, *Appl. Surf. Sci.*, 2012, **258**, 3835.
22 (*a*) Z. Xue, S. Wang, L. Lin, L. Chen, M. Liu, L. Feng and L. Jiang, *Adv. Mater.*, 2011, **23**, 4270; (*b*) K. Ellinas, A. Tserepi and E. Gogolides, *Langmuir*, 2011, **27**, 3960.
23 A. Ahuja, J. A. Taylor, V. Lifton, A. A. Sidorenko, T. R. Salamon, E. J. Lobaton, P. Kolodner and T. N. Krupenkin, *Langmuir*, 2008, **24**, 9.
24 X. Yao, J. Gao, Y. Song and L. Jiang, *Adv. Funct. Mater.*, 2011, **21**, 4270.
25 (*a*) X. Zhu, Z. Zhang, X. Xu, X. Men, J. Yang, X. Zhou and Q. Xue, *J. Colloid Interface Sci.*, 2012, **367**, 443; (*b*) J. Yang, Z. Zhang, X. Men, X. Xu, X. Zhu, X. Zhou and Q. Xue, *J. Colloid Interface Sci.*, 2012, **366**, 191.
26 (*a*) Y. Guo, W. Li, L. Zhu and H. Liu, *Mater. Lett.*, 2012, **72**, 125; (*b*) Jin Yang, Z. Zhang, X. Xu, X. Men, X. Zhu and X. Zhou, *New J. Chem.*, 2011, **35**, 2422.

27 K. Kurogi, H. Yan, H. Mayama and K. Tsujii, *J. Colloid Interface Sci.*, 2007, **312**, 156.
28 T. Darmanin and F. Guittard, *J. Am. Chem. Soc.*, 2011, **133**, 15627.
29 (*a*) M. Wolfs, T. Darmanin and F. Guittard, *Macromolecules*, 2011, **44**, 9286; (*b*) T. Darmanin, E. Taffin de Givenchy and F. Guittard, *Macromolecules*, 2010, **43**, 9365.
30 J. M. Conder, R. A. Hoke, W. de Wolf, M. H. Russell and R. C. Buck, *Environ. Sci. Technol.*, 2008, **42**, 995.
31 M. Houde, J. W. Martin, R. J. Letcher, K. R. Solomon and D. C. G. Muir, *Environ. Sci. Technol.*, 2006, **40**, 3463.
32 J. P. Giesy and K. Kannan, *Environ. Sci. Technol.*, 2001, **35**, 1339.
33 N. Kudo and Y. Kawashima, *J. Toxicol. Sci.*, 2003, **28**, 49.
34 H. H. Zhou, J. B. Wen, X. H. Ning, C. P. Fu, J. H. Chen and Y. F. Kuang, *J. Appl. Polym. Sci.*, 2007, **104**, 458.
35 H. H. Zhou, S. Q. Jiao, J. H. Chen, W. Z. Wei and Y. F. Kuang, *Thin Solid Films*, 2004, **450**, 233.
36 A. Merz, R. Schropp and E. Doetterl, *Synthesis*, 1995, **7**, 795.
37 J. A. Schiffner, T. H. Woeste and M. Oestreich, *Eur. J. Org. Chem.*, 2010, **1**, 174.